UNITED STATES
DEPARTMENT OF THE INTERIOR
U.S. GEOLOGICAL SURVEY

MULTIFRACTALS IN IMAGE PROCESSING AND PROCESS IMAGING

By Lee De Cola

Open-File Report 91-301

Reston, Virginia
1991

ACKNOWLEDGMENTS

I thank Norman Bliss, Pat S. Chavez, Jr., and Nicholas C. Matalas of the U.S. Geological Survey, and Nina Lam, for their helpful comments, and the staff of the U.S. Geological Survey's EROS Data Center in Sioux Falls, South Dakota, for providing imagery. This research was conducted under the auspices of a National Research Council Research Associateship at the U.S. Geological Survey National Center in Reston, Virginia.

CONTENTS

ILLUSTRATIONS

TABLES

MULTIFRACTALS IN IMAGE PROCESSING AND PROCESS IMAGING

Lee De Cola
U.S. Geological Survey
521 National Center
Reston, Virginia 22092

ABSTRACT

Image data may be analyzed for a range of scale levels by generalizing high resolution measurements into an image pyramid whose statistical description is used to estimate a fractal dimension D_t for each value t of the image histogram. This multifractal analysis is demonstrated for a satellite image of Reston, Virginia, which is compared to data simulated by Gaussian and random walk processes. The behavior of the multifractal dimension is used to characterize simulated and empirical data and to detect low- and high-dimension features in the image.

INTRODUCTION

Casual observation, as well as a great deal of empirical research, reveals that

- spatial *phenomena* are complicated and irregular,
- spatial *patterns* tend to be self-similar among scales, and
- spatial *data* cannot be completely characterized using Euclidean notions of points, lines, planes, and volumes.

Fractal sets, which are irregular, self-similar, and non-Euclidean, can be used to analyze data for many kinds of spatial phenomena. This paper presents results from experiments using fractal concepts in the analysis of images. Four kinds of sets—topological, ideal, stochastic, and empirical—can in part be characterized by multiple fractal dimensions D. These measures are applied to empirical data, and the results are then compared to data simulated to mimic spectral characteristics of the real images. This comparison suggests a hierarchy of spatial processes that give empirical data their richness and complexity. Although the

---

Any use of trade, product, or firm names in this publication is for descriptive purposes only and does not imply endorsement by the U.S. Government.

objective of extracting features from images is demonstrated, the exercise also provides a broader understanding of spatial process.

Let us make a distinction among these four kinds of sets, which are not always self-similar across scales or space, and not all of which correspond to a single (monofractal) dimension (De Cola, 1991):

Fractal set	Irregular	Self-similar	Fractal dimension
Topological	No	Yes	Single (integer)
Ideal	Yes	Yes	Single
Stochastic	Yes	Yes	Multiple
Empirical	Yes	No	Multiple

Topological spaces establish the Euclidean framework, usually $\mathbb{R}^3$, within which data are gathered, and may be used to define locations of observations, usually bounded by $\mathbb{R}^1$ lines in $\mathbb{R}^2$. Such topological fractal sets are self-similar and have unique integral nonnegative dimensions $D \in \mathbb{N}$.

Ideal fractal sets illustrate the fundamental ideas of fractal geometry, namely the irregular self-similarity of single-dimension (monofractal) sets. The infinite Koch "snowflake" construction is an example of an ideal fractal set with dimension $D = \log 4/\log 3 \sim 1.26$ identically at all scales, uniformly at all locations, and consistently at all times. Much like their Euclidean counterparts the point, line, or plane, ideal fractals are perfect and unchanging.

Stochastic fractal sets require that we drop the monofractality assumption and measure many dimensions in order to represent the varying form of a phenomenon as a function of local variables across space. These sets, which have a self-similar structure compounded with a random component, are more complex and are particularly useful in the simulation of realistic data. But unlike ideal fractal sets, stochastic data are multifractals whose dimensions change with intensity, location, time, and even across scales. Figure 1, for example, is a rendering of a cellular random walk in two dimensions, where the vertical axis is the number of times a given cell is visited (Kaye, 1989). This simple cellular model generates an irregular self-similar pattern—small pieces look like the whole—yet the pattern can only be characterized as having more than a single (monofractal) dimension (Barnsley, 1988; Falconer, 1990).

Finally, *empirical* fractal data, which represent a decidedly nonfractal world, require that we abandon self-similarity except within a range of scales. Because real spatial phenomena are the products of scale-bound processes, their descriptions vary depending on how, where, and when they are measured. Far from being a liability, this situation means that a measurement such as fractal dimension is a function $D(\ )$ of local variables. Multifractal measurement can be used as a description of how spatial patterns, as well as hypothetical underlying processes,

vary in irregularity at different intensities from place to place and time to time and even among scales. This paper describes how the multifractal model can be used to explore spatial structure and to make inferences about processes in the real world.

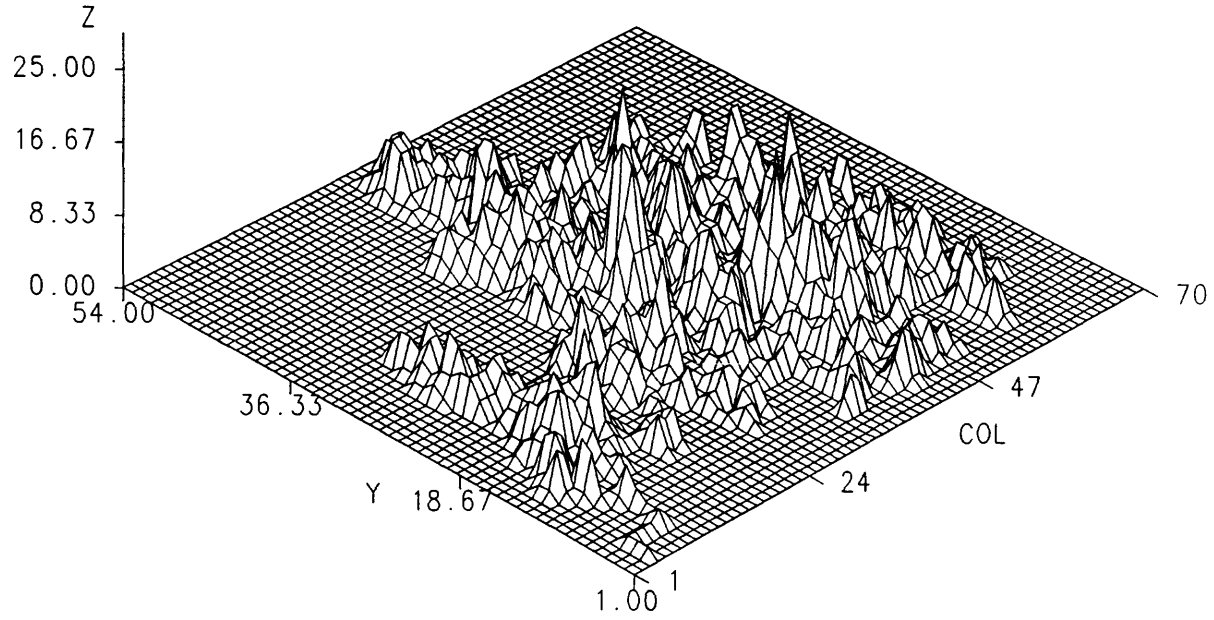

Figure 1.—Three-dimensional rendering of an orthogonal, unit-step, random walk in two dimensions.

The world is therefore not "fractal" in the ideal sense, for the processes underlying real phenomena are too complex to be characterized by any single model (Nicolis and Prigogine, 1989). But empirical data are increasingly amenable to models embodying the fractal paradigm of self-similar irregularity represented over a wide range of scales by nonintegral dimension. It should also be recognized that fractal analysis is just one approach to the measurement of spatial variation; two other multiscale approaches are Fourier and variogram analysis (Roy, 1986; Burrough, 1989). Although there is not enough space here to develop this argument, we can demonstrate that the fractal model is quite robust, parsimonious, and therefore at least as powerful a characterization of spatial data as these alternative techniques.

MULTISCALE ANALYSIS

Before we turn to the application of these ideas to simulated and empirical data, we must establish an algorithmic foundation for the multiscale analysis of spatial form. This foundation is particularly valuable because several approaches to the measurement of fractal dimension exist. We begin with topological specifications that provide data about a phenomenon within some maximum spatial extent and for a smallest resolution element. Let $L > 0$ be an integer with $n = 2^L$ and let X_0 be an $n \times n$ array (raster) of integers representing the value of some variable x_0. One way to generalize this 0-level array is by sampling every

other cell (pixel) in every other row, yielding an $(n/2)\times(n/2)$ array (Justice et al., 1989). The technique used here, however, is to take the mean value of each 2×2 subarray, which generalization may be repeated to yield a stack of L+1 layers X_ℓ, $\ell = 0, \ldots, L$, as shown in Figure 2, for $L = 4$. Each layer in the stack is a generalization of the layer below (Uhr, 1987).

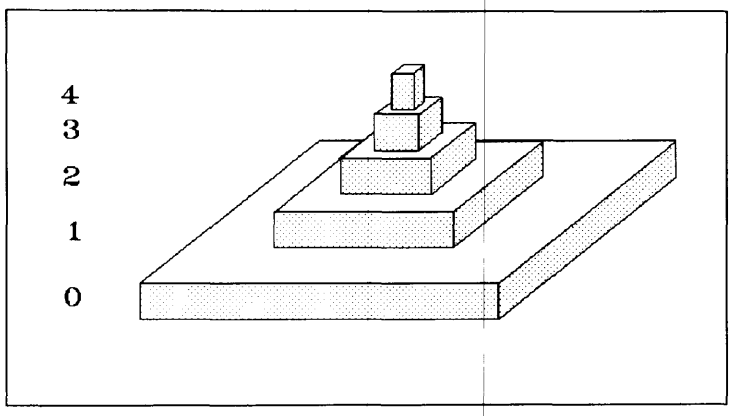

Figure 2.—An L = 4 data pyramid in which each layer is an aggregation of the one below.

Three things should be noted. First, it is possible to use subarrays other than the 2×2 chosen, but this is a natural choice that also allows rapid bit arithmetic. Second, while the size of the original $\ell = 0$ layer is $(2^L)^2$, the size of the complete image pyramid is only $4/3(2^L)^2$. Third, although the size of each layer is one-fourth that of the one below it, the amount of information (as measured, for example, by some qualitative assessment of image "clarity") certainly declines more slowly than this.

The fractal analysis of empirical data is based on the examination of statistics computed at each level. At level $\ell = 0$ let a subset of X_0 be $X_{t0} = \{x_0: x_0 \geq t\}$, where t is a threshold value of the array (threshold brightness in the case of an image) and let e_{t0} be the length of the boundary of X_{t0}, i.e., a count of the cell edges separating X_{t0} from its complement $X_0 \backslash X_{t0}$ (Culling, 1989). It is possible to generalize this measurement to the set $X_{t\ell} = \{x_\ell: x_\ell \geq t\}$ which yields $e_{t\ell}$, the cell boundary of the generalized set $X_{t\ell}$. Fractal dimension is a measure of the scaling relationship between a region's boundary and its scale level ℓ: $e_{t\ell} = a_t(2^\ell)^{-b_t}$ which, taking logs yields

$$\log_2(e_{t\ell}) = \log_2(a_t) - b_t\ell + \varepsilon_t \qquad (1)$$

where ε_t is an ordinary least squares error term. Because the data X exist in the topological 3-dimensional space $[\mathbb{R}^2 \times \mathbb{I}]$ of location × value, $D_t = 3 - b_t$ (Falconer, 1990, p. 42). The regression also yields an estimate of a_t, a measure of size, which will not be discussed here (De Cola, 1989a and 1989b; see Whalley and Orford, 1989, for other approaches).

This multiscale analysis provides not merely a single *mono*fractal D but a *multi*fractal function D_t (Lovejoy and Schertzer, 1988) that varies with the intensity of a phenomenon (in this

case t, the brightness values of an image). The expectation is that $0 \leq D_t \leq 2$; the irregularity of the phenomenon measured by the data X may range between that of a point singularity, for which $D = 0$, and that of a Euclidean set (such as a white disk on a black field) for which $D = 2$. D_t is therefore a tool whereby we can measure the form of a phenomenon across its range and, by selecting different windows, throughout the space it occupies.

A simple way to illustrate these ideas is with a remotely sensed image. The SPOT high-resolution visible (HRV) panchromatic sensor detects energy in the range of 0.45 to 0.80 μm for $(10\text{m})^2$ pixels. Figure 3 shows the location of a SPOT scene chosen for analysis, a 10-level $(10.24\text{ km})^2$ image centered on the USGS National Center in Reston, Virginia. (Permission to use this image courtesy of SPOT Image Corporation, Reston, Virginia © 1990 CNES.) The image (hereinafter called Image, to distinguish it from simulated data) is shown as a pyramid in Figure 4, in which frame 0 is at the highest resolution (1024x1024 pixels of $(10\text{ m})^2$) while frame 1 shows the data aggregated into 512×512 pixels each of $20\times20\text{-m}^2$, and so forth. Note how each scale level, while similar to its neighbors in the pyramid, has its own characteristics. The higher resolution images ($\ell = 0, 1$) are best for the identification of individual features such as lots and roads; middle resolutions ($\ell = 4, 5$) are suitable for the detection of large, complex areas; and low resolutions ($\ell = 8, 9$) highlight broad areas of high and low brightness. A $(10.24\text{ km})^2$ single-pixel, level-10 image could also be regarded as part of an even larger array, in keeping with the idea of movement up an open-ended scale pyramid. (In fact, a number of the frames are similar in resolution, but not necessarily in spectral sensitivity, to such sensors as SPOT multispectral (frame 1), Landsat Thematic Mapper (frame 2), Landsat multispectral (frame 3), Coastal Zone Color Scanner (frame 6), and Advanced Very High Resolution Radiometer (frame 7).)

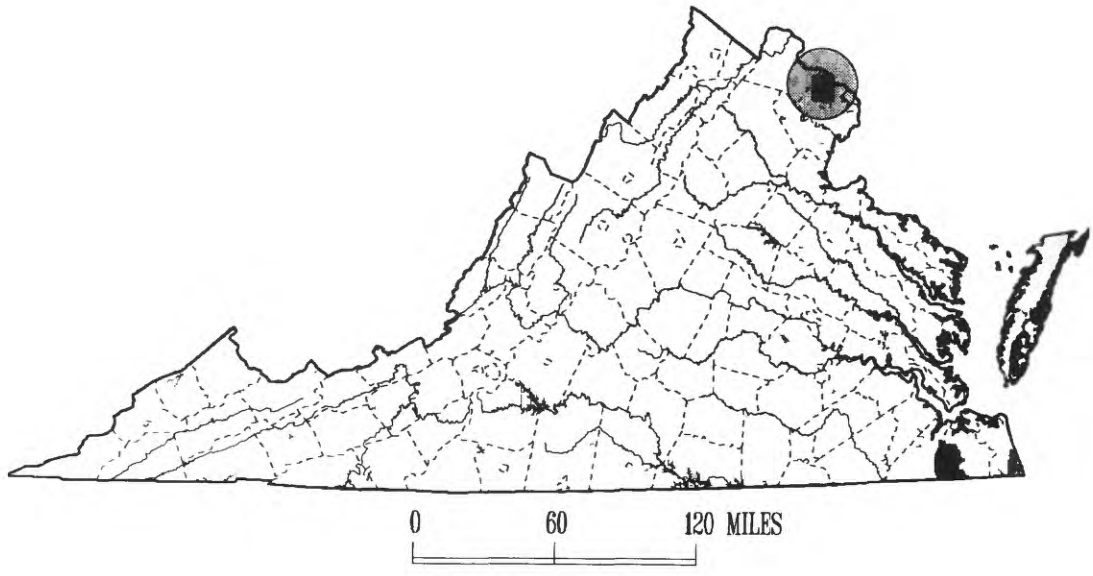

Figure 3. Location of the $(10.24\text{ km})^2$ Reston, Virginia, SPOT scene.

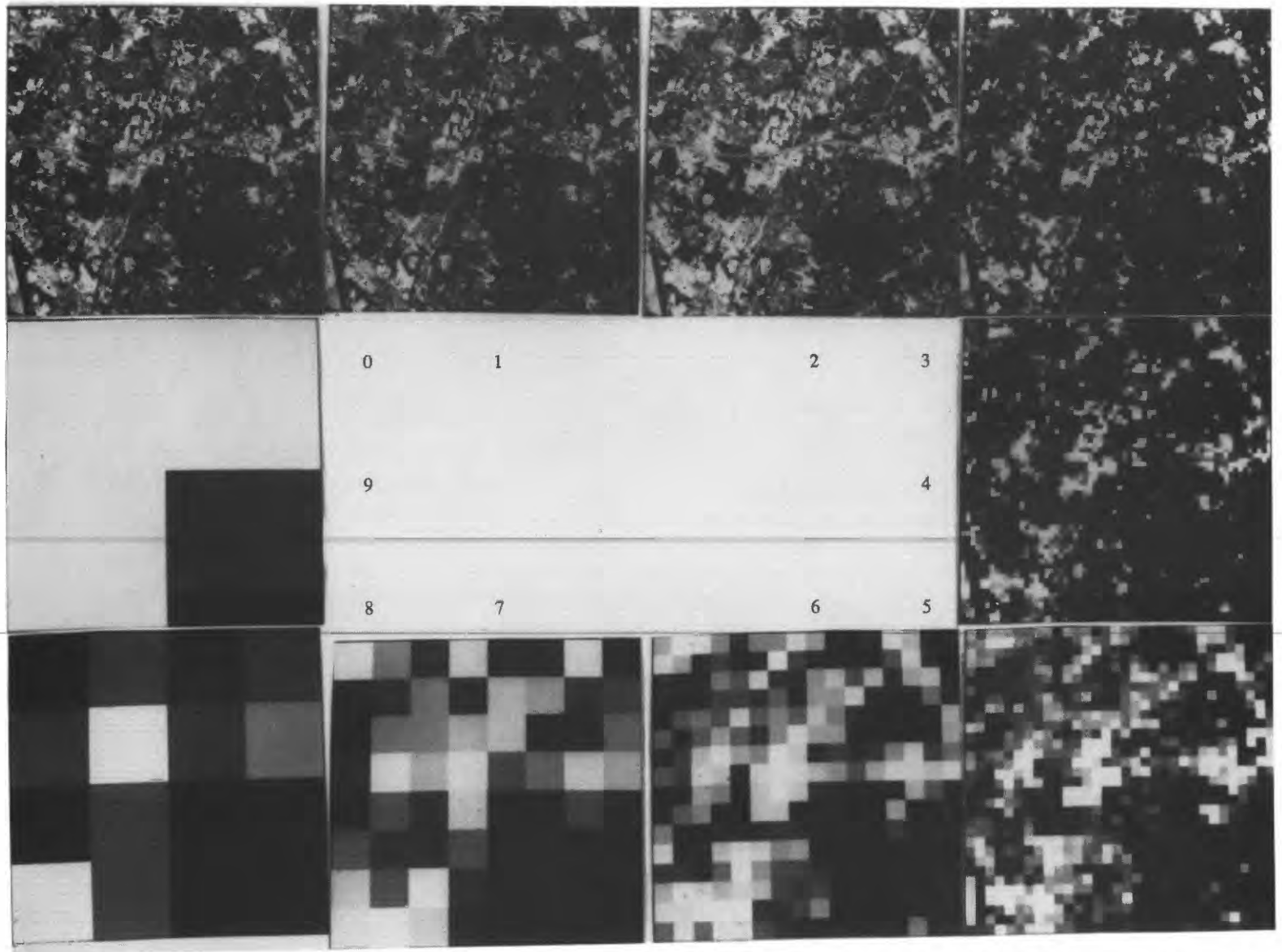

Figure 4.—An L = 10 data pyramid for the Reston, Virginia, image. Frame 0 is the original 1024^2 10-m image, frame 1 is a 512^2 20-m aggregated image, and so on. Each frame is 10.24 km wide.

Table 1 shows the characteristics of this pyramid. Because each layer is an aggregation of the one below it, $\overline{X}_\ell = 46.1$ for $\ell = 0, \ldots, 10$, but the standard deviation of the data s_ℓ declines with scale. Such a data structure, like the related quadtree scheme, allows us to move within the [0, L] continuum of a scale space (Samet, 1990). Upward movement is towards aggregation, large features, and generalization, while downward movement is toward disaggregation, greater detail, and the segmentation of space (Goodchild and Mark, 1987; Hummel, 1987).

Table 1.—Statistics of the data pyramid for the Reston, Virginia, image.

Level ℓ	Edge 2^ℓ	Cell size meters	Number of cells $4^{L-\ell}$	Standard deviation of data s_ℓ
L = 10	1,024	10,240	1	—
9	512	5,120	4	2.17
8	256	2,560	16	2.30
7	128	1,280	64	3.47
6	64	640	256	4.38
5	32	320	1,024	5.65
4	16	160	4,096	6.85
3	8	80	16,384	7.93
2	4	40	65,536	9.09
1	2	20	262,144	9.68
0	1	10	1,048,576	10.21

Figure 5 shows a plot for Image of the values of $\{D_t; t \in [28, 81]\}$, each estimated by using equation (1). (The minimum R^2 for these 54 estimates is 0.95.) Clearly the data are not monofractal: $D_t = 0.402 \pm 0.515$ and these dimensions have a typically multifractal parabolic shape (Falconer, 1990). For low values of t the phenomenon is essentially pointlike, with few edges separating the sparse set from its background complement. Low values of D_t are also found for high values of t, but here the roles of figure and background (set and complement) are reversed. And the maximum $D_{46} = 1.21$, occurs at X. Shown on the figure is a quadratic fit to the data:

$$\hat{D}_t = -2.67 + 0.144t - 0.000177t^2 \qquad R^2 = 0.70 \qquad (2)$$

(where the caret signifies prediction) that gives a predicted maximum of $\hat{D}_{48} = 0.87$. Moreover, there is significant autocorrelation among the values of D_t—the Durbin-Watson statistic = 0.611 ($DW_{.01} = 1.36$), which does not support the hypothesis of nonautocorrelated disturbances (Theil, 1971). Not only is D a parabolic multifractal, each value is correlated with its neighbors, and this should be considered when modeling the behavior of D_t.

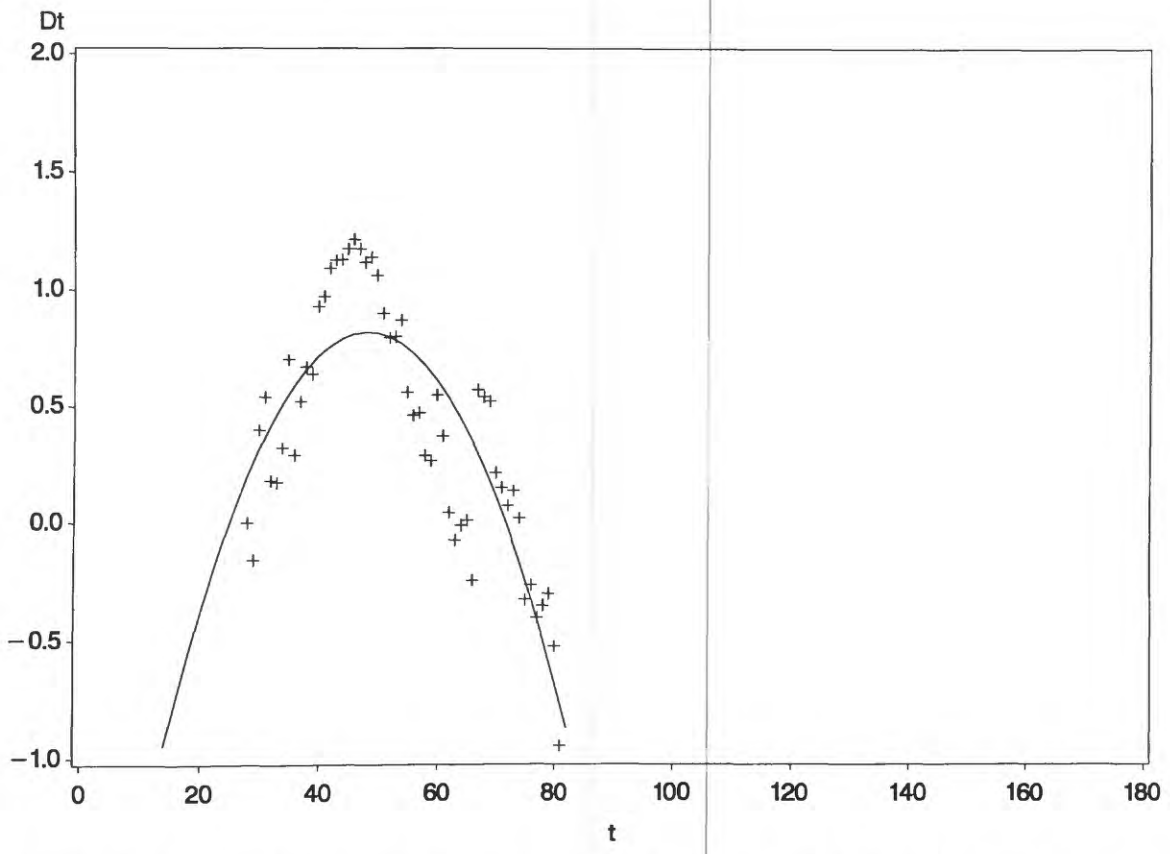

Figure 5. Fractal dimension D_t versus threshold pixel value t for the Reston, Virginia, image, with quadratic fit.

SIMULATION: PROCESS IMAGING

To better understand what D_t tells us about Image, it will be useful to explore how D_t behaves for data over whose parameters we have some control. While the objective of image *processing* is often simply to improve the appearance of an image in some way, the more ambitious task of digital image *analysis* is to make inferences about the real world based on the information from raster data (Muller, 1988). For example, the 10^7 bits of the X_0 Image are reduced to the three coefficients of equation (2) relating D_t to t—a mere 10^2 bits—a good example of data reduction. Of course a great deal of data are lost in this process, but we gain information for inferences about the processes that might have given rise to the image.

To consider what fractal analysis has revealed about the Image data, we need to explore alternative spatial processes that might give rise to such an array of numbers. This approach to spatial process modeling may be called "process imaging." This technique, which is a form of visualization but more explicitly deductive, reverses the direction of image processing by producing large data sets from relatively brief descriptions of spatial process consisting of a few instructions. For example, the 10^2 bits that specify the first two moments of the Image

data will be used to simulate an image of 10^7 bits, a good example of data expansion (Frenkel, 1988).

Consider therefore what processes might simulate various aspects of the Image data whose mean $\overline{X} = 46.1$ and standard deviation $s = 10.2$. Figure 6 shows one way of organizing a class of cellular spatial models according to whether or not they manifest three characteristics:

- Are the values of a cell *quantities* (numerical measurements) as opposed to nominal classes, as in a raster GIS? An example of a quantitative process would be the Poisson model of the completely random location of points among cells (Schachter and Ahuja, 1979; De Cola, 1991).

- Are all values determined *simultaneously* or sequentially over some period? Cellular automata are examples of processes in which array values are computed across space at the same time (Wolfram, 1984; Phipps, 1988).

- Is the value of one cell *autocorrelated* with (affected by the value of) any other cell? Diffusion limited aggregation is an example of a process that sequentially assigns a nominal binary value to a cell based on the values of its neighbor (Batty et al., 1989).

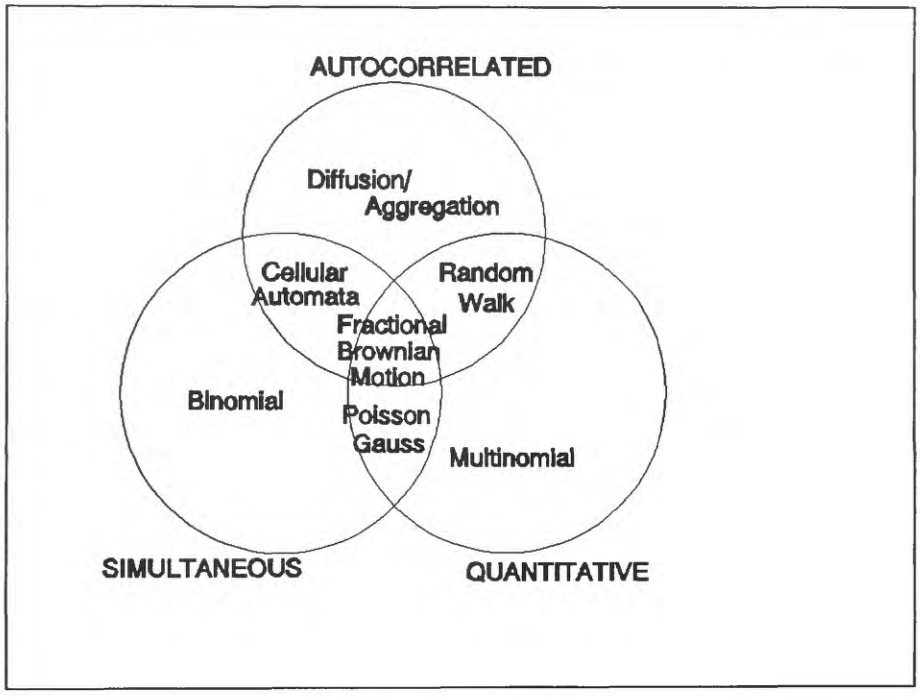

Figure 6. A typology of cellular processes according to whether they have three characteristics.

These characteristics may be combined in various ways to provide a wide range of hybrid models for the study of a given real-world phenomenon. Perhaps the most useful such hybrid is fractional Brownian motion (Musgrave et al., 1989), but there are many other examples.

To reproduce certain characteristics of the Image data, we have used two relatively simple processes, called Gauss and Randomwalk, to simulate images of 256^2 pixels each. The simplest simulation of the image is a "heap" of pixels whose spectrum is normally distributed with the same mean and standard deviation as the Image. (Think of taking the pixels from Image, scrambling them, and then withdrawing a smaller set of 65,536 pixels.) Figure 7 shows one such simulation, and although Gauss and Image share the first two moments of their histograms, their appearance is very different. The complete entropy of the Gauss reveals virtually no spatial information. In fact, this image is one representation of what an absolutely fractal world might look like: stochastically identical at all scales and no cues about the size or location of anything.

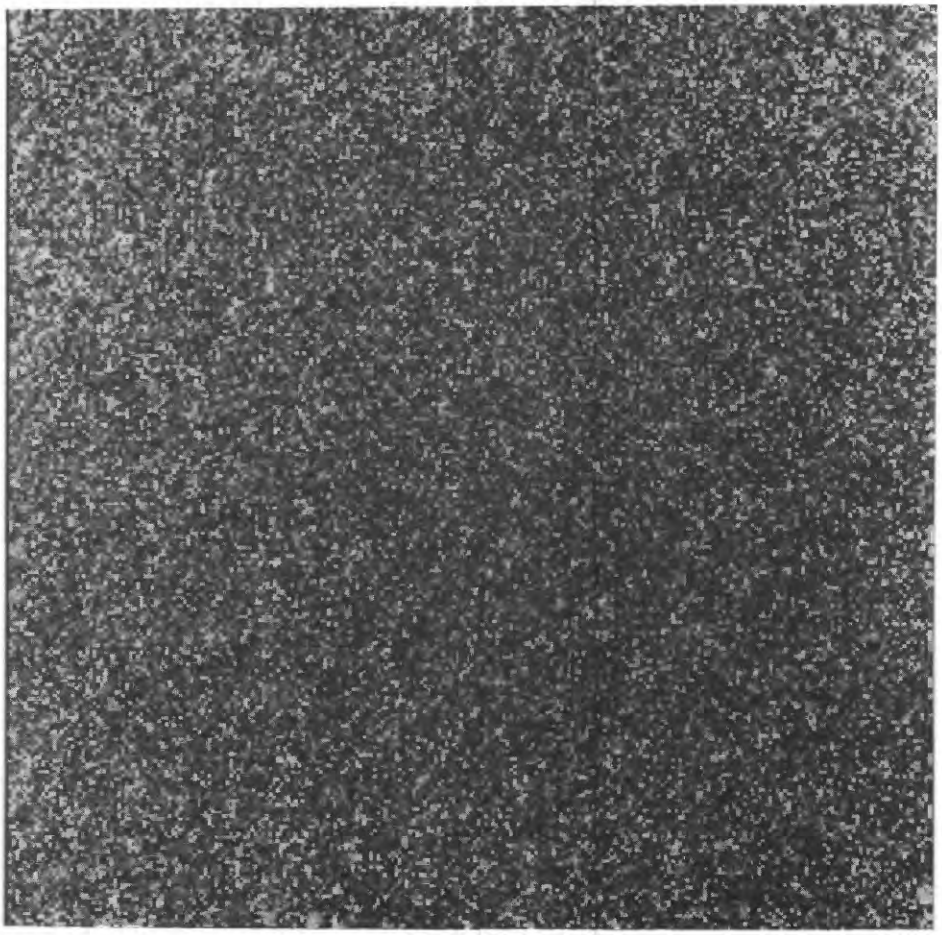

Figure 7. Gauss simulation on a 256^2 array using the same mean and standard deviation as the Reston, Virginia, image.

The Gauss model is the most parsimonious way to simulate raster data spectrally similar to a given image. The problem is that this process manifests no spatial autocorrelation because the value of each cell is unrelated to that of any other. This totally random behavior is indicated in Figure 8 by the fact that the estimation of D_t is confined to a very narrow range of the image values, $38 \leq t \leq 55$, centered on the mean of the image histogram, although $x_0 \in [4, 86]$. Moreover, $D_t < 0$ for all but three values of t. This behavior appears to reflect the extreme spatial dispersion of the Gauss process, where spatial autocorrelation is absent, clusters of homogeneous pixels are rare, and therefore the dimensionality of the process is low (the possibility of negative multifractal dimensions is discussed in Mandelbrot, 1989). Certainly this process corresponds neither in appearance nor in process to the real world.

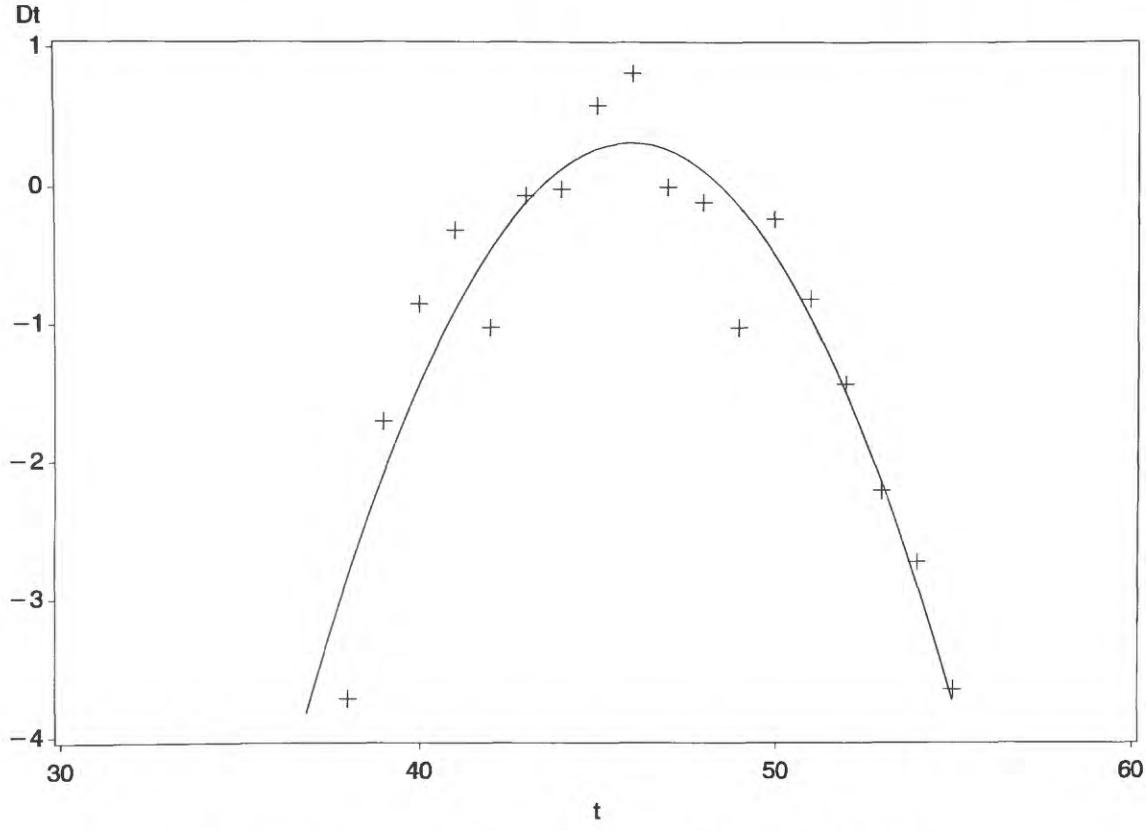

Figure 8. Fractal dimensions for a Gauss simulation.

It is illuminating to compare the Gauss simulations to a spatial process shown in the typology of Figure 6 that *is* clearly autocorrelated. We simulated 16 random walks that begin with a square lattice window of 256^2 empty cells, i.e. $x_0 = 0 \; \forall \; x$, starting at the central cell. The simulation moves randomly according to the uniform distribution of $Pr(\uparrow) = Pr(\downarrow) = Pr(\rightarrow) = Pr(\leftarrow) = \frac{1}{4}$. Each time a cell is visited, the value of x_0 is incremented and the process stops when $\Sigma x_0 = \bar{X} \times 256^2 = 46.1 \times 65{,}536 = 3{,}020{,}554$ steps. If the process leaves one edge of the array it returns at the opposite edge, so that a unit-step orthogonal random walk on a torus is simulated (De Cola, 1991). An example of this simulation is shown in Figure 9.

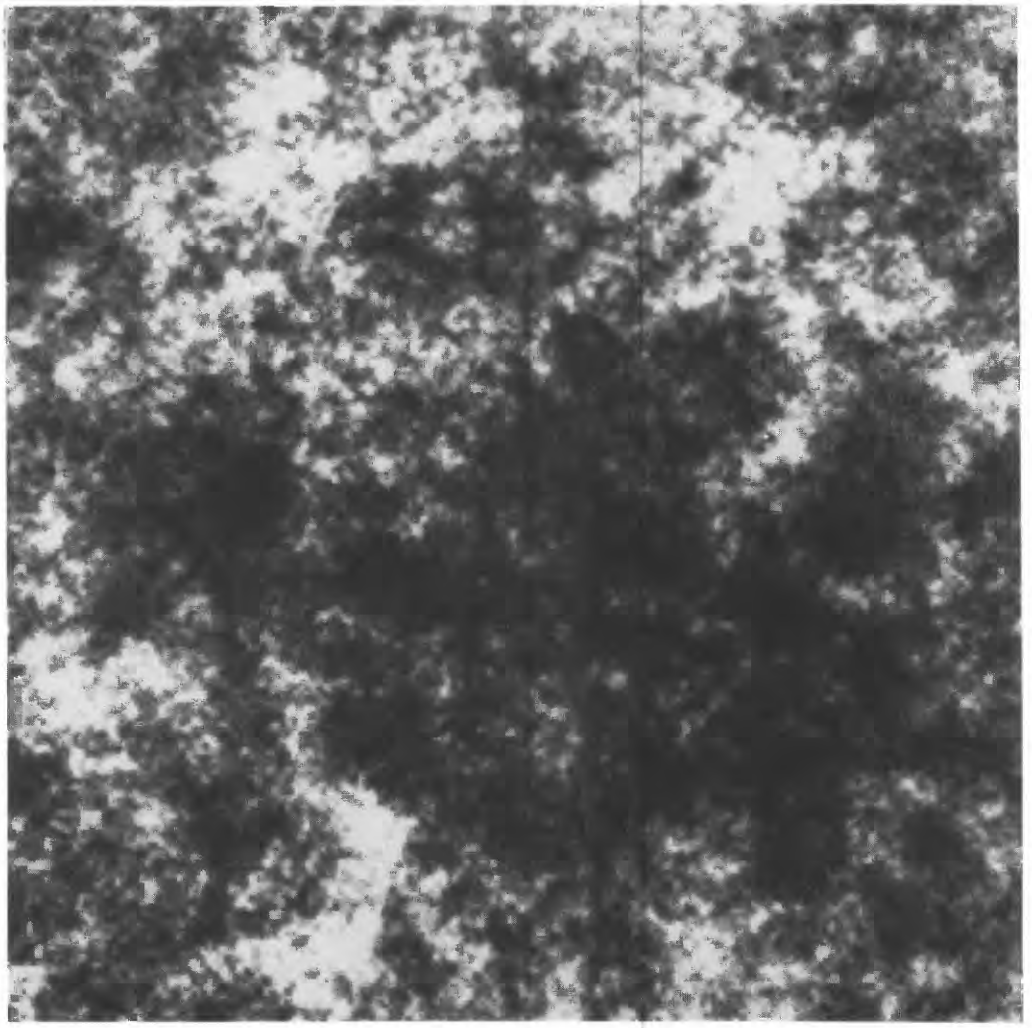

Figure 9. Randomwalk simulation on a 256^2 lattice, with the same mean as the Reston, Virginia, image.

The Randomwalk simulation corresponds to the Image data if we imagine that the brightness values for each pixel are numbers representing events at $(10\ m)^2$ locations; indeed, the radiance values are linear and homogeneous transformations of the energy received within the frequency limits of the sensor (SPOT, 1988). Although the simulation shown in Figure 9 might be an adequate representation of cloud data (Joseph, 1985) or perhaps chaotic terrain (Goodchild, 1982; Jones et al., 1989), it bears only weak resemblance to the study image but is certainly closer than Gauss. The fractal plot of this simulation, shown in Figure 10, is also different from that of the Gauss process. The process yields a characteristic parabola, but the curve spans a wider domain and range than Gauss. Even for low values of brightness the

image gives a wide range of dimensions, generally in the range $0 \le D_t \le 1.3$. When fitted to a quadratic polynomial, the simulation yields

$$\hat{D}_t = -0.328 + 0.0519t - 0.000481t^2 \qquad R^2 = 0.65$$

which has a predicted maximum $\hat{D}_{54} = 1.07$. Although these results share the parabolic shape of the Gauss process, much more acceptable dimensions are produced and for a much larger domain of t values (compare Figures 5 and 8).

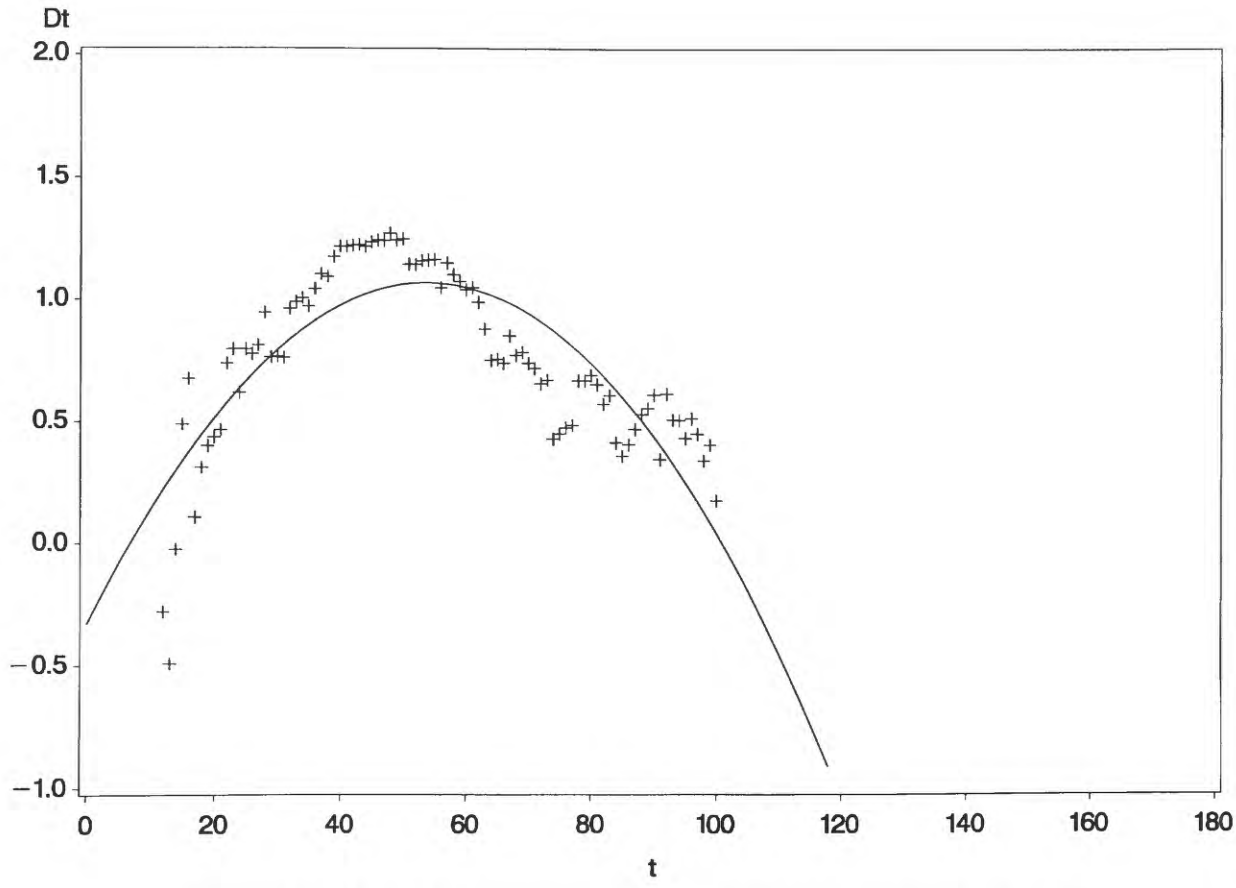

Figure 10. Fractal dimensions for a single Randomwalk simulation.

So far the analysis has been largely visual and qualitative. Two stochastic processes (Gauss and Randomwalk) and one empirical data set (Image) have similar histograms, but give very different images. While the behavior of D_t for each of the three has been shown to have the parabolic form typical of multifractal sets, the domain of dimension for Gauss is too restricted and its range too frequently negative to be an appropriate model for the empirical image. We may therefore abandon Gauss as a model and pursue Randomwalk. To examine the general behavior of Image over space and to provide data with a sufficient sample size, we divided the full 1024×1024-pixel image into sixteen 256×256-pixel subwindows and computed D_t for

each value of t for each subwindow. Figure 11 represents a fractal plot of the results. D_t spans almost all of its expected range, and although this scatter has no particular mathematical form, a cubic polynomial has been plotted to suggest that the data may have an underlying parabolic shape significantly distorted by a third-degree term at the positive extreme.

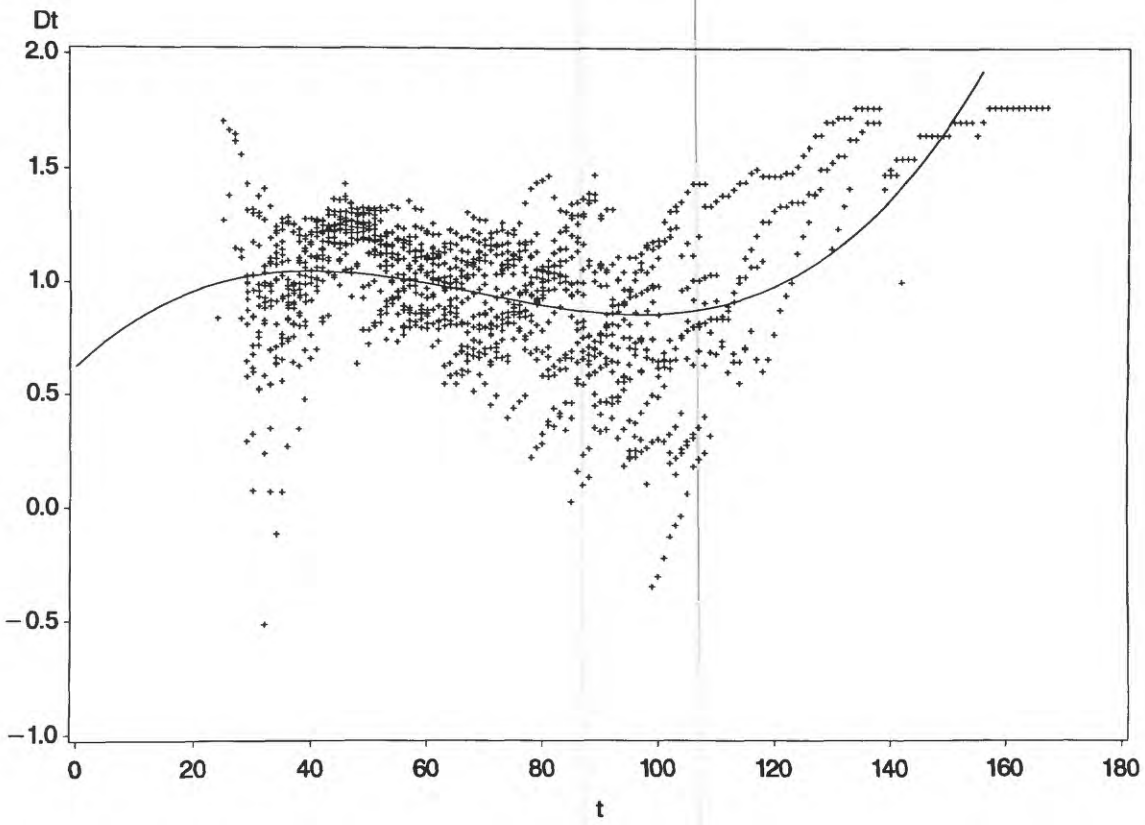

Figure 11. Fractal dimensions for sixteen 256×256-pixel subwindows of the Reston, Virginia, image, with cubic fit.

Using the mean of the image histogram, 16 Randomwalk simulations were also run. Their fractal plot (Figure 12) indicates that the cubic polynomial gives a better fit. Table 2 displays the results of fitting third-order polynomials to the relationship between D_t and t for the two sets of 16 images. Terms were added to the model if they were statistically $\neq 0$ at the 10 percent level of significance. The table, as well as a comparison of Figures 11 and 12, reveals similarities among and differences between the 16 Randomwalk simulations and the 16 subwindows of Image. On the one hand, both roughly correspond to a cubic polynomial, the estimates of whose terms (except for the intercept) differ by no more than 10 percent. On the other hand, the two data sets differ in the following ways: (1) Randomwalk corresponds to a cubic relationship in all but two of the simulations, while the results of Image subwindows are less consistent; (2) the distributions of all of the Image coefficients are highly and inconsistently skewed; and (3) the mean R^2 for the Randomwalk regressions is over 50

percent higher than that for Image. (A curve such as $D_t = \alpha t^{\beta} e^{\gamma t}$, with a maximum at $t = -\beta/\gamma$, might better fit the Image results. A similar curve appears in Mandelbrot, (1989).)

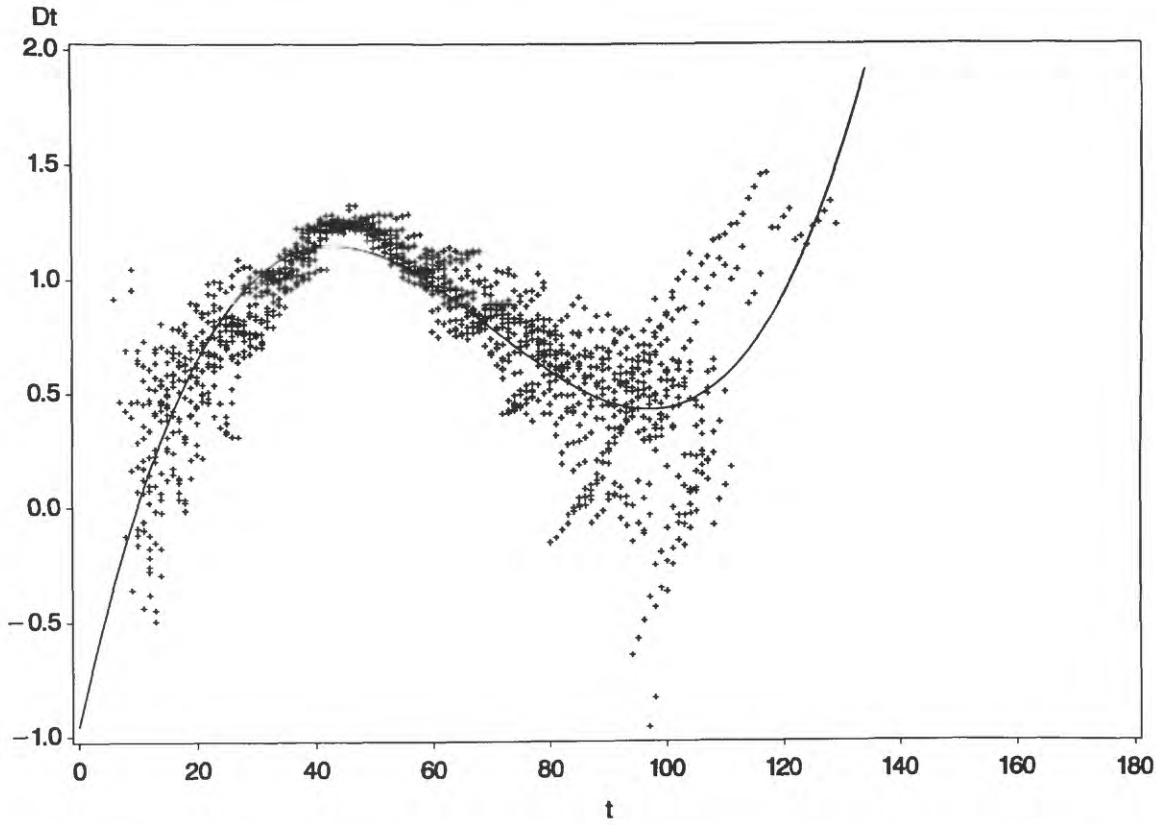

Figure 12. Fractal dimension for sixteen Randomwalk simulations on a 256^2 lattice.

Table 2. Results of fitting third degree polynomials to the 16 Randomwalk and 16 Image subwindows.

	Random walk 16 simulations				Image 16 subwindows			
Term	N	Mean	Standard deviation	Skewness	N	Mean	Standard deviation	Skewness
0	16	-0.749	0.579	-0.661	16	-0.515	2.41	-1.275
1	16	0.0915	0.0336	0.871	13	0.0930	0.128	1.230
2	16	-0.00138	0.000626	-0.654	14	-0.00127	0.00206	-1.502
3	14	0.00000665	0.00000315	0.561	12	0.00000633	0.0000120	1.288
R^2	16	0.774	0.0802	-0.468	16	0.507	0.206	-0.289

FROM IMAGE TO MAP

These experiments suggest that multifractal dimensions reflect different characteristics of spatial process. In general, $\partial^2 D_t / \partial t^2 < 0$, and D_t may have complex behavior for autocorrelated processes. We have observed that, although the mean values of the three processes (Gauss, Randomwalk, and Image) are the same and their histograms are all roughly normal, their spatial appearances (and consequently their fractal behavior) are quite different. Gauss is a diffuse multifractal whose lack of spatial autocorrelation results in largely negative values of D_t. Randomwalk is a spatially coherent stochastic multifractal for which $D_t = 0.76 \pm 0.38$, varying with intensity. The subimages of Image are real multifractals for which $D_t = 0.98 \pm 0.33$, varying not only with intensity but also strongly with location; i.e., the spatial form of a given brightness value is a function not only of (possibly inherent) *processes* associated with the data but also of *where* the value occurs. In keeping with the above notion of multifractals, it therefore appears that combinations or hierarchies of models will be necessary to explain real spatial patterns (Getis and Boots, 1978). Certainly we have had to abandon the monodimensional restriction of ideal fractal sets.

In fact, the spatial variation of the Image process may be seen by examining a particular layer of the data pyramid. At $\ell = 5$, for example, there are $(2^{(10-5)})^2 = 1024$ subwindows, each of which has an ensemble of associated multifractal dimensions. Figure 13 maps the values of $D_{43} = 1.28 \pm 0.313$. We can see exactly how D_t varies over space, and in fact, this picture could be viewed as a fractal of a fractal, or "metafractal." Whether or not this is a suitable neologism, the figure is a clear illustration of how far this real-world phenomenon deviates from the isotropism of ideal fractality. The process appears to be stationary, however, as fitting the data to a plane reveals no significant north-south or east-west trend.

Any automated technique designed to extract features from images must be sensitive to dependencies upon intensity and location in spatial pattern. The above exercise illustrates moreover that considerable intelligence—natural as well as artificial—is necessary to interpret spatial and spectral information (Uhr, 1987). Because fractal concepts provide a key to the multiscale measurement of self-similar spatial patterns, it is possible to use scale information to distinguish among patterns in real-world images. Dimension can be used to spatially identify features in a way that suggests how automated image processing based on multiscale analysis might work.

We have used the technique developed here to do some image processing on a subwindow of Image, specifically a 256×256-pixel subwindow around the South Lakes region of the scene (Figure 14). A parabolic fit to the multifractal dimensions of this image gives the equation

$$\hat{D}_t = 1.107 + .00887t - .000130t^2 \qquad R^2 = .72$$

Figure 15 shows the residuals $\hat{\varepsilon}_t = (D_t - \hat{D}_t)$ from this regression. Consider first the maximum residual $\hat{\varepsilon}_{27} = .27$, implying that the values of the image for $t \geq 27$ have a more regular boundary than do other thresholds. When the values of the image $x_0 \leq 27$ are colored black,

as in Figure 16, we see that they are associated with the lakes of the region. Another interesting interval is defined by $47 \leq x_0 \leq 57$, the longest run of negative residuals (i.e., relatively low dimensional features whose perimeters quickly disappear at higher scales). When the pixels associated with this interval are colored gray, we see in Figure 16 that they may be associated with some of the roads in the subwindow. We therefore arrive at a crude thematic map of the region, created by using a semiautomated technique that can be used to extract other features as well.

The above distinction among fractal processes consequently applies to extracting information—and ultimately making maps—from images. Although the relatively scale-independent structure of the Randomwalk model can be used to characterize the fractal behavior of the Image data, some of the interesting natural and cultural features we wish to highlight in a map are revealed by the extent to which they deviate from simulated processes. It is useful to speculate on other processes that might have given rise to the patterns in which we are interested to see why the exceptions that make the world so interesting actually occur, particularly as a result of human activity. Indeed, the detection and depiction of these exceptions are one of the main functions of the mapping process.

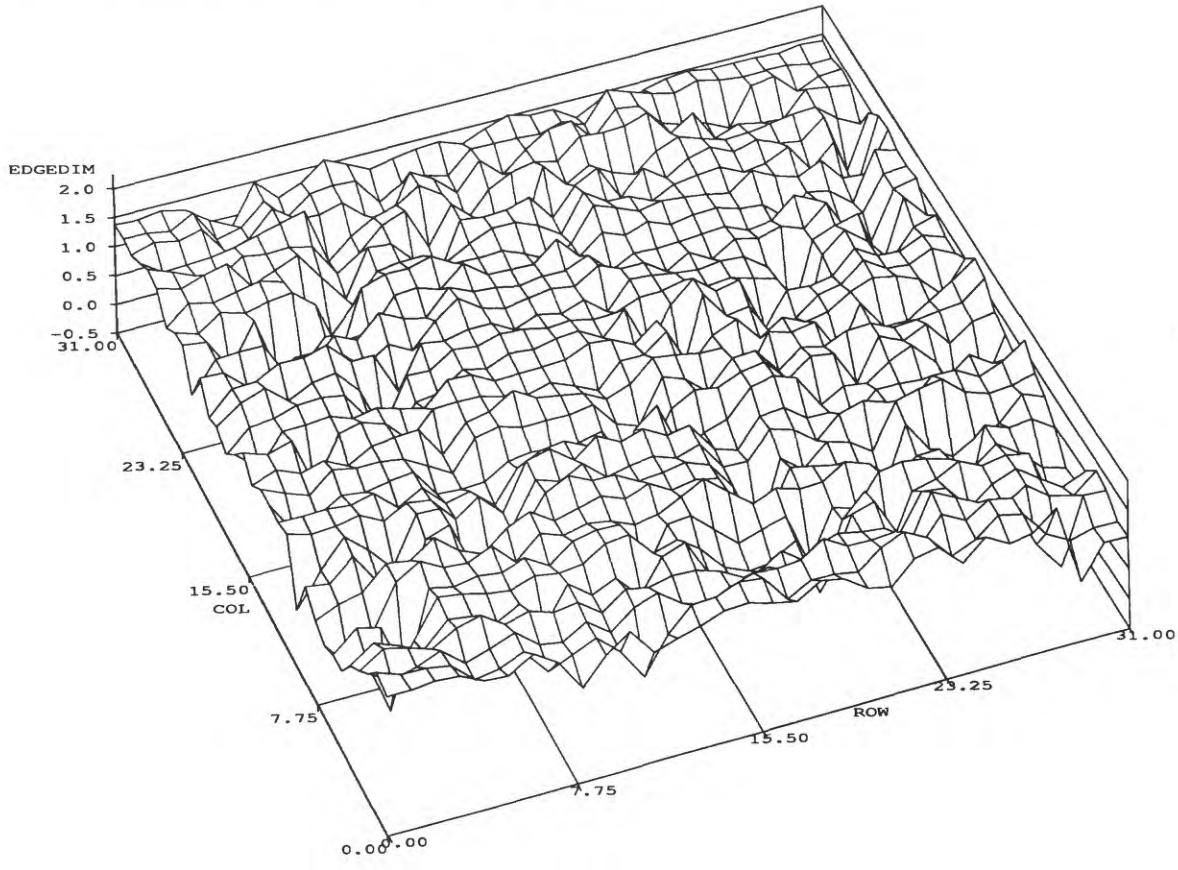

Figure 13. Three-dimensional plot of the values of D_{43} for 1024 (= 32×32) subwindows of the Reston, Virginia, image.

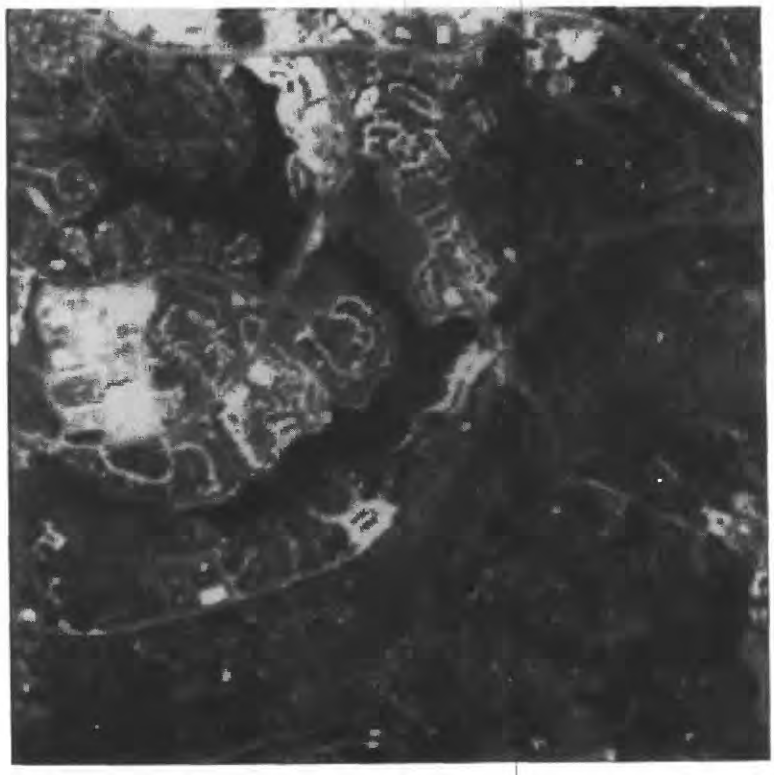

Figure 14. Panchromatic image of the South Lakes subwindow of the Reston Image.

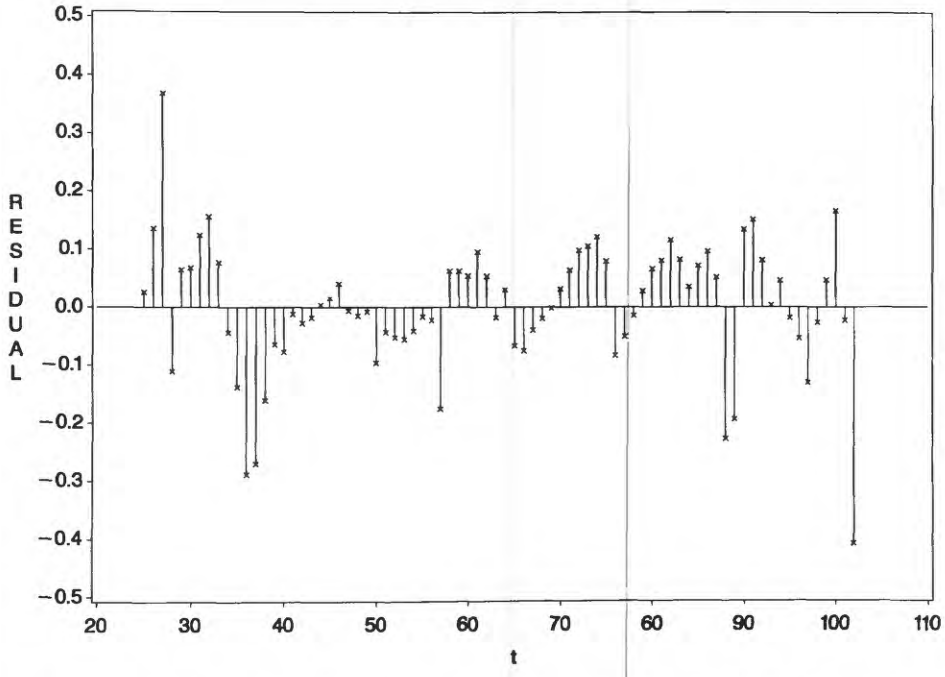

Figure 15. Residuals from quadratic fit of D_t for South Lakes subwindow.

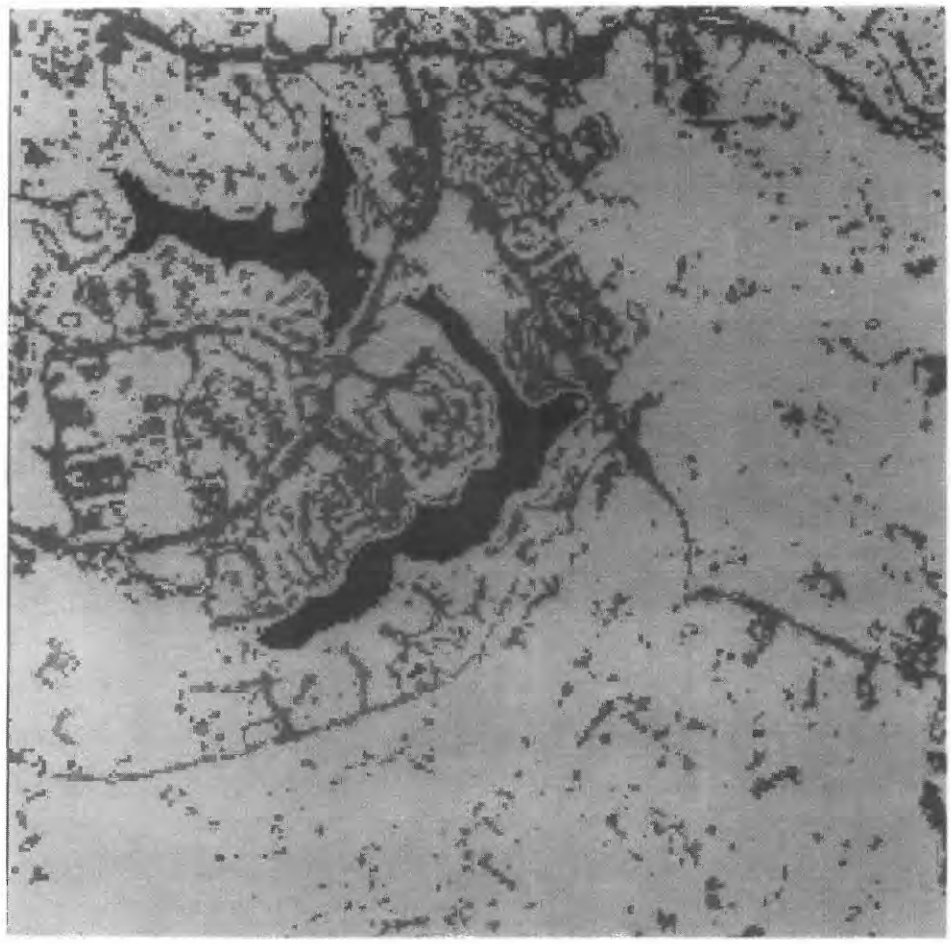

Figure 16. The South Lakes subwindow classified into high-dimension "lakes" and low-dimension "roads."

CONCLUSION

On the basis of the above results, we may therefore postulate that four kinds of models coexist in the real world:

- true *noise*, like that of Gauss, that is often inherent in instruments and is completely scale independent,
- more complex *physical* processes that can often be visualized by stochastic models (like that of Randomwalk), which in the real world look like mountains and clouds and result from generally chaotic processes that are relatively scale independent,
- *natural* processes, such as vegetation and other land cover evolution, that are the result of complex multifractal systems working within relatively narrow scales, and finally,

- *cultural* or human activities that are frequently erratic, difficult to predict, and often strikingly scale dependent.

The analysis has also illustrated how movement within a scale space allows a scientist to aggregate or subdivide space in order to focus at will on low-level measurement, high-level description, and feature detection. Those phenomena that are more scale independent (closer to the classical fractal ideal) require fewer data than others whose scale and location dependence reveal exceptions. This approach is obviously of value for the management of data, and extends the notion of the quadtree by asserting the pertinence of *all* scales of the image pyramid to the understanding of process (Samet, 1990). No level is universally appropriate for examination; each reveals important scale dependencies, and taken together, all may be used both to summarize the irregularity of pattern and to make inferences about the complexity of process. While it is obviously true that the level-0 image contains all the data that exist, higher level images are more suitable for more generalized analysis, and from a data management perspective, they are considerably smaller.

The analysis also suggests the value of simulation and visualization in image analysis. The notion of *process modeling* includes and extends specific techniques of image processing and land use classification to encompass broad multidisciplinary studies that analyze varieties of data to make complex inferences about real-world processes (Holdridge et al., 1971; Szeliski and Terzopoulos, 1989; Schlesinger et al., 1990). Spatial scientists are beginning to merge sophisticated multivariate analytical techniques with the manipulation of image data, and we need to acquire skills in this area that are commensurate with our integral-dimension (point-arc-polygon) capabilities. We are also witnessing a convergence between image processing, which ideally reduces large amounts of data to smaller amounts of information, and process imaging, which produces large amounts of data from the information contained within small models. A dialectic between these techniques is developing.

Finally, this exercise has demonstrated how multifractal analysis of spatial data can be used to make inferences about the processes that give rise to spatial patterns. The techniques of remote sensing and geographic information system analysis are being extended by a wide range of disciplines (Holden, 1988; Chrisman, 1990). Such fields as geophysics, geomorphology, hydrology, geology, and economic geography provide a rich set of spatial models with predictions of spatial pattern that have been associated not merely with specific fractal dimensions, but with multifractal behavior. It is clear that we have only just begun to make use of a powerful idea that enables us to reach beyond the concepts and techniques of any one discipline.

REFERENCES

Barnsley, M.F., 1988, Fractals everywhere: San Diego, Academic Press.

Batty, M., Fotheringham, A.S., and Longley, P., 1989, Urban growth and form: scaling, fractal geometry, and diffusion-limited aggregation: Environment and Planning A, v. 21, p. 1447-1472.

Burrough, P.A., 1989, Fractals and geochemistry *in* Avnir, D., ed., The fractal approach to heterogeneous chemistry: surfaces, colloids, polymers: New York, Wiley.

Chrisman, N.R., 1990, Review *of* Building databases for global science: Annals of Association of American Geographers, v. 80, no. 1, p. 149-151.

Culling, W.E.H., 1989, The characterization of regular/irregular surfaces in the soil-covered landscape by gaussian random fields: Computers & Geosciences, v. 15, no. 2, p. 219-226.

De Cola, Lee, 1989a, Fractal analysis of a classified Landsat scene: Photogrammetric Engineering and Remote Sensing, v. 55, no. 5, p. 601-610.

_____ 1989b, Pareto and fractal description of regions from a binomial lattice: Geographical Analysis, v. 21, no. 1, p. 74-81.

_____ 1991, Fractal analysis of multiscale spatial autocorrelation among point data: Environment and Planning A, v. 23.

Falconer, K.J., 1990, Fractal geometry: mathematical foundations and applications: New York, Wiley.

Frenkel, K.A., 1988, The art and science of visualizing data: Communications of the ACM, v. 31, no. 2, p. 111-121.

Getis, Arthur, and Boots, Barry, 1978, Models of spatial process: Cambridge, Cambridge University Press.

Goodchild, M.F., 1982, The fractional brownian process as a terrain simulation model: Modeling and Simulation, v. 13, p. 1133-1137.

Goodchild, M.F., and Mark, D.M., 1987, The fractal nature of geographic phenomena: Annals of the Association of American Geographers, v. 77, p. 265-278.

Holden, Constance, 1988, The ecosystem and human behavior: Science, v. 242, p. 663.

Holdridge, L.R., Grenke, W.C., Hatheway, W.H., Liang, T., and Tosi, J.S., Jr., 1971, Forest environments in tropical life zones: a pilot study: Oxford, Pergamon.

Hummel, R., 1987, The scale-space formulation of pyramid data structures *in* Uhr, Leonard, ed., Parallel computer vision: Orlando, Fla., Academic Press, p. 107-124.

Jones, J.G., Thomas, R.W., and Earwicher, P.G., 1989, Fractal properties of computer-generated and natural geophysical data: Computers & Geosciences, v. 15, p. 227-235.

Joseph, J.H., 1985, Morphology of fair weather cumulus cloud fields as remotely sensed from satellites, and some applications: Advances in Space Research, v. 5, no. 6, p. 213-216.

Justice, C.O., Markham, B.L., Townshend, J.R.G., and Kennard, R.L., 1989, Spatial degradation of satellite data: International Journal of Remote Sensing, v. 10, no. 9, p. 1539-1561.

Kaye, Brian, 1989, A random walk through fractal dimensions: New York, VCH Publications.

Lovejoy, S., and Schertzer, D., 1988, Extreme variability, scaling and fractals in remote sensing: analysis and simulation *in* Muller, J.P., ed., Digital image processing: Philadelphia, Taylor & Francis, p. 177-212.

Mandelbrot, B.B., 1989, Negative fractal dimensions and multifractals: Physica A, v. 163, p. 306-315.

Muller, J.P., ed., 1988, Digital image processing: Philadelphia, Taylor & Francis.

Musgrave, F. K., Kolm, C.E., and Mace, R.S., 1989, The synthesis and rendering of eroded fractal terrains: Computer Graphics, v. 23, no. 3, p. 41-50.

Nicolis, Gregoire, and Prigogine, Ilya, 1989, Exploring complexity: New York, Freeman.

Phipps, Michel, 1988, Dynamical behaviour of cellular automata under the constraint of neighbourhood coherence: Geographical Analysis, v. 21, no. 3, p. 197-215.

Samet, Hanan, 1990, The design and analysis of spatial data structures: Reading, Mass., Addison-Wesley.

Schachter, B., and Ahuja, N., 1979, Random pattern generation processes: Computer Graphics and Image Processing, v. 10, p. 95-114.

Schlesinger, W.H., Reynolds, J.F., Cunningham, G.L., Huenneke, L.F., Jarrell, W.M., Virginia, R.A., and Whitford, W.G., 1990, Biological feedbacks in global desertification: Science, v. 247, p. 1043-1048.

SPOT Image Corporation, 1988, SPOT User's Handbook: Reston, Va.: SPOT Image Corp.

Szeliski, Richard, and Terzopoulos, Demitri, 1989, From splines to fractals: Computer Graphics, v. 23, no. 3, p. 51-60.

Theil, H., 1971, Principles of econometrics: New York, Wiley.

Uhr, Leonard, ed., 1987, Parallel computer vision: Orlando, Fla., Academic Press.

Whalley, W.B., and Orford, J.D., 1989, The use of fractals and pseudofractals in the analysis of two-dimensional outlines: review and further exploration: Computers & Geosciences, v. 15, no. 2, p. 185-197.

Wolfram, S., 1984, Cellular automata as models of complexity: Nature, v. 31, no. 4, p. 419-424.